The Extraordinary Equatorial Atlantic Warming in Late 2019

Richter, Ingo
Application Laboratory, JAMSTEC

Tokinaga, Hiroki
Research Institute for Applied Mechanics, Kyushu University

Yuko M. Okumura
Institute for Geophysics, Jackson School of Geosciences, University of Texas at Austin

出版情報：Geophysical Research Letters. 49 (4), pp.e2021GL095918-, 2022-02-21. AGU
バージョン：

Geophysical Research Letters

RESEARCH LETTER
10.1029/2021GL095918

The Extraordinary Equatorial Atlantic Warming in Late 2019

Ingo Richter[1], Hiroki Tokinaga[2], and Yuko M. Okumura[3]

[1]Application Laboratory, JAMSTEC, Yokohama, Japan, [2]Research Institute for Applied Mechanics, Kyushu University, Kasuga, Japan, [3]Institute for Geophysics, Jackson School of Geosciences, University of Texas at Austin, Austin, TX, USA

Key Points:

- One of the strongest equatorial Atlantic warm events of the last 40 years developed in late 2019
- Wind stress forcing both on and off the equator contributed to the exceptionally strong warming
- Analysis suggests that remote forcing from other basins was not a major factor in the genesis of the event

Supporting Information:

Supporting Information may be found in the online version of this article.

Correspondence to:

I. Richter,
richter@jamstec.go.jp

Citation:

Richter, I., Tokinaga, H., & Okumura, Y. M. (2022). The extraordinary equatorial Atlantic warming in late 2019. *Geophysical Research Letters*, *49*, e2021GL095918. https://doi.org/10.1029/2021GL095918

Received 2 SEP 2021
Accepted 29 JAN 2022

Abstract Sea-surface temperatures (SSTs) in the eastern equatorial Atlantic are subject to variability on interannual timescales but during the last 20 years, this variability has shown comparatively little activity. In late 2019, however, the warmest event in the satellite observation period developed. Analysis suggests that zonal wind stress anomalies in the western equatorial Atlantic contributed to the development of the warm SST anomalies. Furthermore, wind stress curl anomalies north of the equator generated downwelling Rossby waves that propagated to the western boundary and were reflected into downwelling Kelvin waves that helped to precondition the event. Neither the contemporaneous positive Indian Ocean Dipole nor the El Niño Modoki appears to have contributed substantially to the Atlantic warming, though some uncertainty remains. Based on large-scale multidecadal variability patterns, a return to enhanced variability is not imminent but careful monitoring will be important.

Plain Language Summary Year-to-year variability of ocean surface temperatures in the eastern equatorial Atlantic has been relatively weak over the last 20 years. In late 2019, however, an exceptionally strong event developed. This event appears to have been generated by surface wind stress forcing both on and north of the equator. Remote influences from other tropical basins do not seem to have played a large role. Based on large-scale multidecadal variability patterns in the region, the equatorial Atlantic may return to relatively low variability but continued monitoring will be important.

1. Introduction

The equatorial Atlantic is marked by interannual variations in sea-surface temperatures (SSTs) that influence rainfall over the surrounding continents, particularly over West Africa. Early studies emphasized the similarity of this variability pattern with El Niño-Southern Oscillation (ENSO) in the Pacific, and the phenomenon was therefore dubbed "Atlantic Niño" (Merle, 1980). The similarities include SST anomalies that are most pronounced in the eastern half of the basin, and the role of the Bjerknes feedback (Bjerknes, 1969), in which equatorial SST anomalies induce changes in equatorial surface winds that further amplify the pattern. Subsequent research, however, identified several differences with ENSO, including the relatively weak role of the Bjerknes feedback (Nnamchi et al., 2021; Richter et al., 2017) and a strong influence from off-equatorial processes in some events (Foltz & McPhaden, 2010; Lübbecke & McPhaden, 2012; Richter et al., 2013). Partly motivated by these differences, the term "Atlantic Zonal Mode" (AZM) has gained traction in recent years and will be used in the present study.

The AZM is phased-locked to the seasonal cycle (e.g., Keenlyside & Latif, 2007; Richter et al., 2017; Nnamchi et al., 2021), with a primary variability peak in boreal summer (JJA) and a secondary one in boreal winter (NDJ; named AZM II by Okumura & Xie, 2006), as shown by the composites in Figure 1a. It should be noted that this timing can vary considerably for individual events, as pointed out by Vallès-Casanova et al. (2020).

Typical positive AZM events begin with a relaxation of the equatorial trades followed by a deepening of the thermocline and SST warming (and vice versa for negative AZM events; e.g., Richter & Tokinaga, 2021; Vallès-Casanova et al., 2020). Some warm events, however, are preceded by a strengthening of the equatorial trades (Richter et al., 2013). This behavior has been linked to negative wind stress curl anomalies north of the equator, which excite downwelling Rossby waves that are reflected into equatorial Kelvin waves at the western boundary (Burmeister et al., 2016; Foltz & McPhaden, 2010; Lübbecke & McPhaden, 2012).

From about 2000 onward, variability in the equatorial Atlantic has been relatively low (Prigent et al., 2020; Figure S1 in Supporting Information S1). This quiescent period has been attributed to a weaker Bjerknes feedback and stronger latent heat flux damping (Prigent et al., 2020), the latter being partially associated with the strengthening

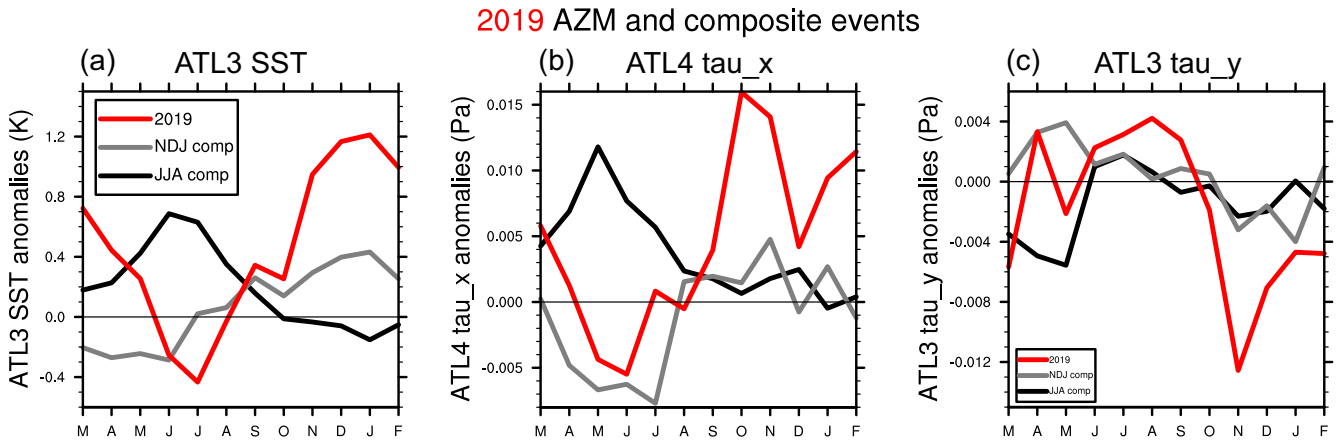

Figure 1. Evolution from March through February of the following year of (a) OISST v2.1 SST anomalies (K) in the ATL3, (b) surface zonal wind stress anomalies (Pa) in the ATL4, and (c) surface meridional wind stress (Pa) in the ATL3. The lines in each panel show a composite summertime AZM (black), a composite AZM II (gray line), and the 2019 event (red line). All anomalies are with respect to the 1988–2017 base period.

of the trade winds over recent decades (Servain et al., 2014). A decrease in equatorial Atlantic SST variability was also found for the period 1950–2009 by Tokinaga and Xie (2011). Contrary to Servain et al. (2014) and Prigent et al. (2020), they found a relaxation of the equatorial trades and the associated thermocline deepening to be responsible for the reduced SST variability. The opposing trade wind trends found in those studies may be partially attributable to the different study periods but also emphasize the uncertainty in observational wind products.

Just as it seemed that the 2000s and 2010s would end without any major AZM event, late 2019 saw the development of an exceptionally strong event (Figure 1 and Figure S1 in Supporting Information S1) that may have been the warmest in the last 40 years (Figure S2a in Supporting Information S1). Another pronounced warm event developed in the summer of 2021 and continued until the end of the year. This raises the question whether the AZM may become more active again, thereby defying projected trends. As a first step to address this question, here we examine the generation mechanism of the 2019 event, put it into the context of previous events, investigate the reasons for its exceptional strength, and discuss possible implications for AZM variability in the coming decades.

2. Materials and Methods

Our SST data set is the Optimally Interpolated SST (OISST), version 2.1 (Huang et al., 2021). Most wind fields used are from the ERA5 atmospheric reanalysis, with additional surface wind stress products from GODAS, NCEP/NCAR reanalysis (Kistler et al., 2001), and the Japanese 55-year Reanalysis (JRA55; Kobayashi et al., 2015). Precipitation is from the Global Precipitation Climatology Project (GPCP), version 2.3 (Adler et al., 2003). The GODAS reanalysis is used for an ocean heat budget analysis. Subsurface in situ observations from the PIRATA moored array (Bourles et al., 2019) are used in the form of the enhanced PIRATA (ePIRATA) data set (Foltz et al., 2018). The satellite sea-surface heights are from AVISO. Interpolated outgoing longwave radiation (OLR) from NOAA satellites (Liebmann & Smith, 1996) are used to investigate remote influences.

Anomalies are calculated as deviations from the climatological cycle for the period 1988–2017 and linearly detrended over the analysis period. For the few datasets that do not reach back to 1988 (namely, ePIRATA [1997-present], and AVISO [1993-present]), we use the beginning of the record up to 2017 as the base period.

The composite positive events in Figure 1 were calculated from years in which the ATL3 index (defined as SST averaged over 20°W-0°E, 3°S-3°N) exceeds 0.8 standard deviations in the JJA average (AZM; years 1984, 1988, 1991, 1995, 1996, 1999, 2007, 2008) or in the NDJ average (AZM II; years 1981, 1987, 1993, 1997, 2003, 2007).

3. Results

3.1. Putting the 2019 Event Into Context

The 2019 AZM event developed in late 2019 and peaked in January 2020 (red line in Figure 1a). It can therefore be classified as an AZM II event (or a late-onset event in the terminology of Vallès-Casanova et al., 2020). From about June 2019 through October, its evolution in the ATL3 region qualitatively followed that of the composite AZM II event (gray line in Figure 1a), but, from October onward, it developed more rapidly and attained an amplitude of 1.2 K, three times higher than the composite AZM II, and 0.5 K higher than the composite summertime AZM (black line in Figure 1a; also Figure S3a in Supporting Information S1). The impression that 2019 was exceptionally strong is supported by comparing 9 observational and reanalysis products from 1982 onward (Figure S2a in Supporting Information S1). Six datasets rank the 2019 event as the strongest (OISST v2.1, HadISST, COBE2, ERA-5, GODAS, and ePIRATA), one data set rates it as the second strongest after 1988 (ERSST), and two rank it as the fourth strongest (ICOADS and OISST v2.0).

3.2. Evolution of the 2019 AZM Event

Up to and including October 2019, SST anomalies in the tropical Atlantic were weak (Figure 2), though some positive anomalies could be seen off southwest Africa in the Angola-Benguela area from July (not shown). The rapid increase from October to November (Figures 1a and 2) was preceded by westerly wind stress anomalies in the ATL4 (45°W-20°W, 3°S-3°N) with a peak of about 0.015 Pa in October (Figures 1b and 2 and Figure S2c in Supporting Information S1), which is unusually strong for this time of the year and, in fact, the strongest westerly anomaly since 1979 (Figure S3b). Both the composite AZM II event and 2019 show pronounced easterlies in early summer that decay toward fall but only 2019 develops pronounced westerlies afterward (Figure 1b).

While the westerly anomalies in 2019 were substantial, they were quite comparable to those during the developing phase of summertime AZM events in MAM (Figure S3b in Supporting Information S1) and do not appear sufficient to explain the exceptional strength of the 2019 event. This indicates that other factors must have contributed.

The rapid warming in October and November was not limited to the equator but extended southward to most of the southern subtropical Atlantic. Particularly warm SST along the southwest African coast indicates the occurrence of a Benguela Niño, which may have partially contributed to the equatorial wind anomalies (Hu & Huang, 2007; Imbol Koungue et al., 2021). We note, however, that there are basin-scale surface wind anomalies from September through November that suggest the involvement of a large-scale process. The wind anomalies are consistent with a weakening of the St. Helena high, which has been found to link AZM and Benguela events (Nnamchi et al., 2016; Lübbecke et al., 2010; Richter et al., 2010). North of the equator, cold SST anomalies weakened the meridional gradient of sea-level pressure, which was associated with cross-equatorial winds and a southward shift of the Atlantic ITCZ that continued into February.

We note that precipitation anomalies over land were rather inconsistent during the event, with the exception of dry anomalies over the coastal region of equatorial Africa. Over South America, a north-south dipole of precipitation anomalies was prominent in November and December but its sign reversed in January and February of 2020.

From February onward, SST anomalies in the ATL3 started decaying (Figures 1 and 2) and were close to zero in April (Figure S2b in Supporting Information S1). While anomalies on the equator weakened in February, warm anomalies off the equator were still relatively strong (Figure 2f).

3.3. Generation Mechanism

The westerly wind anomalies in October suggest a straightforward generation mechanism in which downwelling equatorial Kelvin waves deepen the thermocline and reduce upwelling-induced cooling. Daily mean anomalies of the 20C-isotherm from ePIRATA confirm a substantial deepening of the thermocline, with a peak of almost 30m at the 0 N 0 E mooring in late November (Figure S4). This deepening progresses from west to east, as shown by the buoys at 0 N 23 W, 0 N 10 W, and 0 N 0 E, with positive anomalies commencing in mid-October. The 0 N 35 W buoy, on the other hand, appears to evolve independently, and this is consistent with the wind anomalies in October being strongest east of 30°W (Figure 2).

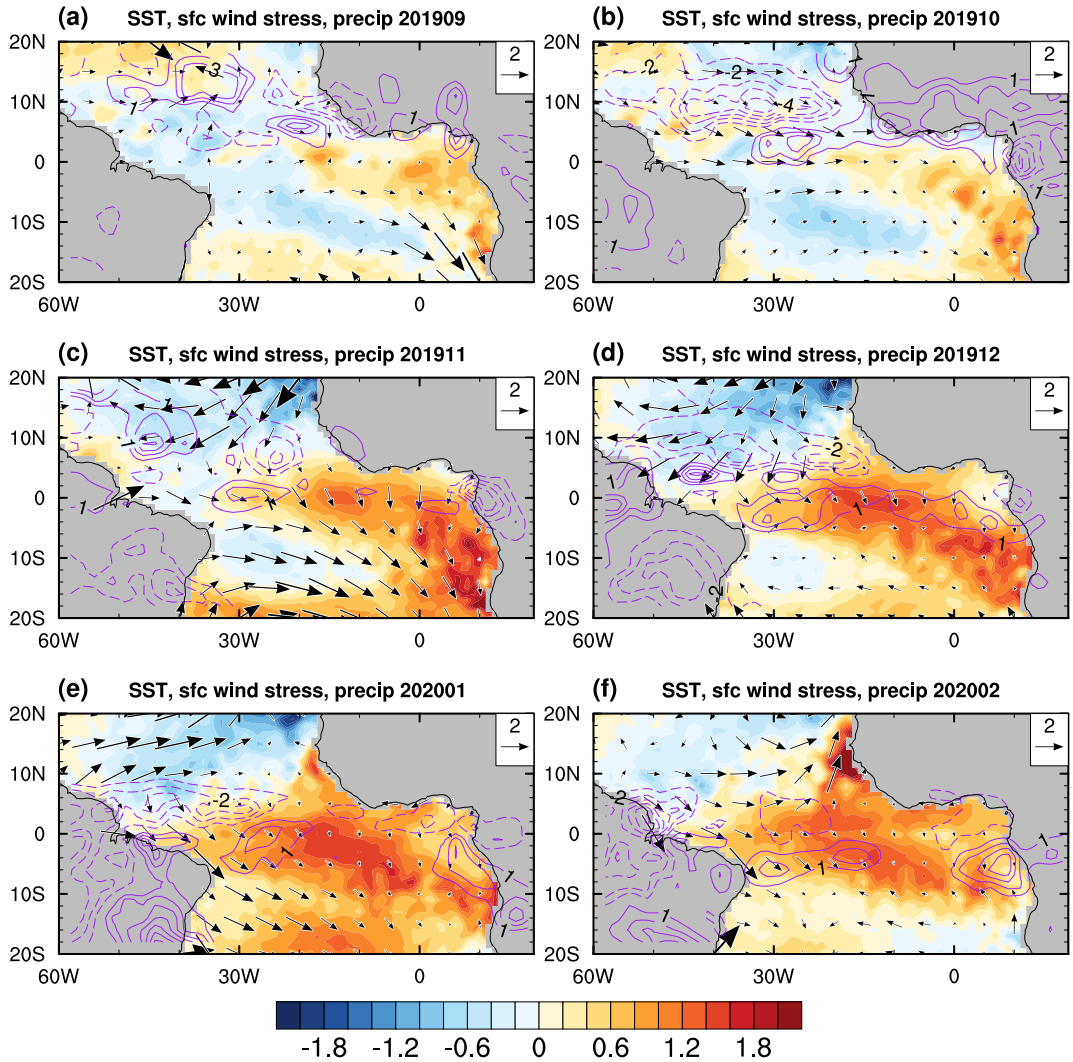

Figure 2. Evolution of the 2019 event from September 2019 through February 2020. Each panel shows anomalies of OISST SST (shading; K), ERA-5 surface wind stress (vectors; reference = 2 Pa*0.01), and GPCP precipitation (contours; interval 1 mm/day; negative contours dashed, 0-contour omitted). All anomalies are with respect to the 1988–2017 base period.

Depth-time sections of ocean temperature from the PIRATA buoys (Figure 3) show that, from spring to early summer, there were cold temperature anomalies in the eastern equatorial Atlantic, though these were mostly confined to the subsurface. From late summer to fall, subsurface temperatures were close to neutral, followed by the rapid development of the 2019 event. Maximum temperature anomalies exceeded 2K at 60m, which is below the mixed layer but above both the climatological and the actual thermocline depth.

Analysis of the GODAS reanalysis suggests that vertical advection dominated the warming below the base of the mixed layer (Figure 4). This is consistent with the westerly wind stress forcing in the western equatorial Atlantic during fall (Figure 2). It should be noted, however, that vertical advection is most pronounced in boreal summer (not shown) when the equatorial wind stress forcing is weak. This may indicate limitations of the reanalysis product but could also be associated with remote influences from the northern equatorial Atlantic, as discussed below. Figures 1c and 2 also suggest that there were pronounced meridional wind anomalies over the ATL3 region, indicating that meridional current convergence may have contributed to local downwelling anomalies and warming (e.g., Okumura & Xie, 2004). The analysis of the meridional current convergence, however, proved to be inconclusive (not shown).

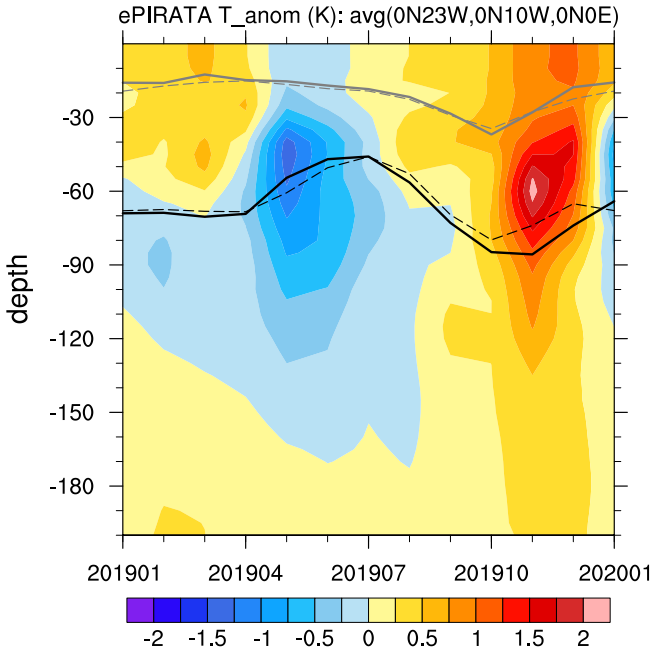

Figure 3. Depth-time section of monthly mean ocean temperature anomalies (shading; K) averaged over the three PIRATA moorings in the ATL3 region (0°N 23°W; 0°N 10°W; 0°N 0°E). The solid gray and black lines show the depth of the mixed layer (defined through a density criterion; see Foltz et al., 2018) and the 20C isotherm, respectively. The corresponding dashed lines show the climatological depths. The base period is 1999–2017.

Analysis of AVISO daily sea-surface height (SSH) anomalies (Figure 5) provides some evidence for westward propagation of positive SSH anomalies north of the equator (Figure 5a; note that the *x*-axis is reversed), consistent with Rossby waves. The waves appear to originate around 10°W from April through June. The Ekman pumping velocity calculated from the ERA-5 reanalysis (Figure S5 in Supporting Information S1) suggests that the local surface wind stress curl generated these downwelling Rossby waves. They appear to be reflected into downwelling Kelvin waves at the western boundary from August through October (Figure 5b) and reach the ATL3 region a few weeks later, where they contributed to preconditioning the 2019 event.

4. Discussion

4.1. Remote Forcing From the Indian and Pacific Oceans

Recent studies have suggested that the tropical Indian Ocean may influence the development of AZM events through changes in the Walker circulation (Liao & Wang, 2021; Zhang & Han, 2021). The 2019 AZM event roughly co-occurred with one of the strongest Indian Ocean Dipole (IOD; Doi et al., 2020; Saji et al., 1999) events on record. The accompanying warming in the western tropical Indian Ocean led to strong precipitation anomalies in October and November (Figure S6 in Supporting Information S1). While the timing of these convective anomalies seems too late to have played a role in the build-up of the 2019 AZM event, a contribution to the rapid development of the AZM from October to November cannot be ruled out. The analysis of outgoing longwave radiation (OLR) anomalies and ERA5 upper-level zonal winds, however, does not provide strong evidence for westward propagation from the equatorial Indian Ocean to the Atlantic (Figures S7 and S8 in Supporting Information S1), neither does the examination of anomalies in the monthly mean Walker circulation (Figure S9 in Supporting Information S1). Thus, there is no strong support for an important role of the Indian Ocean in the 2019 AZM event.

Additionally, there was an El Niño Modoki event in 2019 (Ashok et al., 2007; Doi et al., 2020), which may have influenced the equatorial Atlantic. The analysis of Kelvin wave propagation (Figure S8a in Supporting Information S1), however, does not show major influences on the pronounced equatorial Atlantic westerlies in October.

Overall, it appears, that the 2019 AZM was not strongly influenced by the tropical Indian Ocean or Pacific. It should be noted, however, that OLR may not be able to track disturbances over dry continental regions, and that the reanalysis winds may not be well constrained. It is therefore possible that the actual remote influences were stronger than our analysis suggests. Dedicated GCM experiments may be able to shine more light on the Indian and Pacific Ocean influences.

4.2. Implications for Equatorial Atlantic Variability in the Coming Decades

Both Tokinaga and Xie (2011) and Prigent et al. (2020) point to a weakening of equatorial Atlantic SST variability in recent decades, and climate models tend to project a further decrease in variability, though confidence in these projections is undermined by model biases (Richter & Tokinaga, 2020) and high intermodel variations. It is therefore an interesting question, whether the 2019 AZM event was but a brief flicker or the harbinger of a trend reversal, the latter supported by the subsequent major warm event in 2021.

The cross-equatorial SST gradient is an aspect of the background state that has a large influence on the position of the ITCZ (e.g., Servain et al., 1999), which in turn modulates the strength of coupled feedbacks on the equator (Nnamchi et al., 2021; Richter et al., 2017; Zebiak & Cane, 1987). It is also linked to the state of the Atlantic Multidecadal Oscillation (Martin-Rey et al., 2018; see the Supplementary Information for more discussion on the AMO). More specifically, when SSTs south of the equator are relatively warm, the ITCZ and associated deep convection are located closer to the equator, which strengthens air-sea coupling. Figure S10 in Supporting

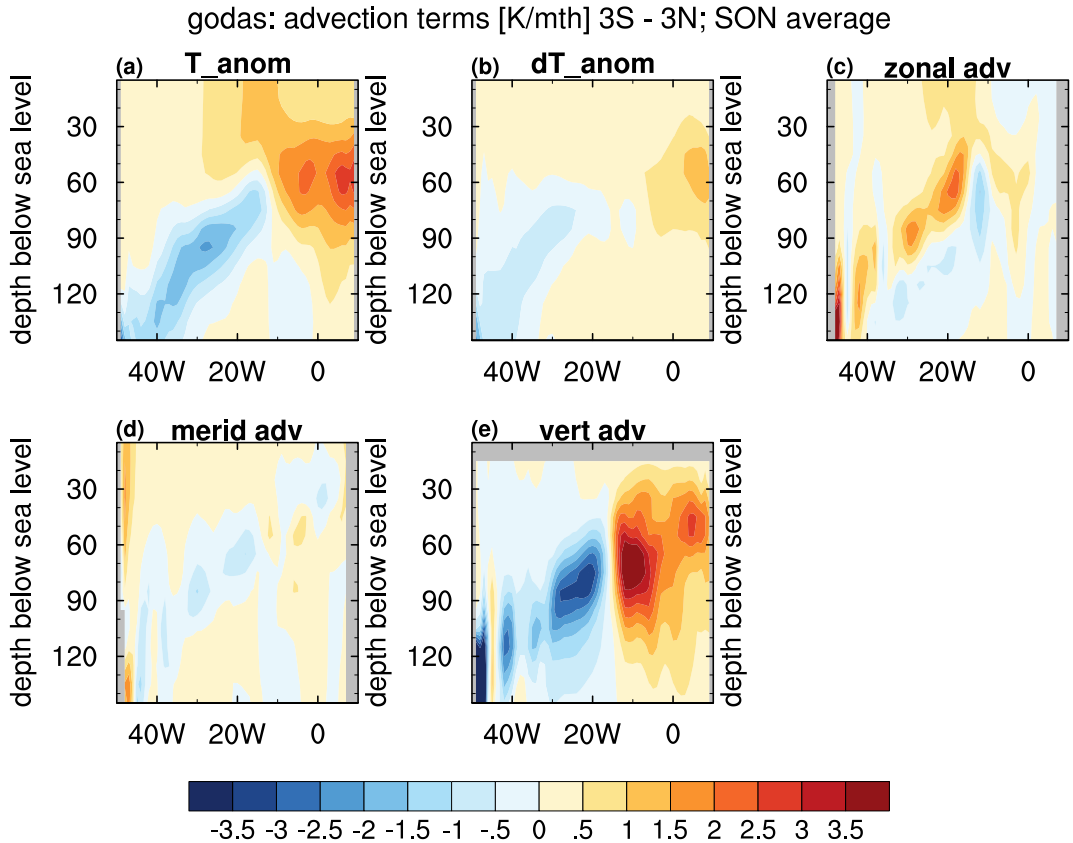

Figure 4. Longitude-depth sections of terms relevant to the oceanic heat budget, meridionally averaged from 3°S to 3°N, and seasonally averaged over September-October-November (SON). The individual panel shows (a) temperature, (b) temperature tendency, (c) zonal advection, (d) meridional advection, and (e) vertical advection. The units are K/month, except for (a), which is in (k) All terms are derived from the GODAS ocean reanalysis. The base period is 1988–2017.

Information S1 shows the difference between south-equatorial SSTs (40°W-10°W, 8°S-2°S) and north-equatorial SSTs (40°W-10°W, 2°N-8°N). This index has moderately low values from approximately 1940 to 1960, high values from 1960 to 1990, and very low values from 1990 onward. This roughly aligns with the periods of high and low variability in the equatorial Atlantic, though a much more detailed analysis would be needed to confirm a physical relation. Nevertheless, based on the meridional SST gradient, a trend reversal is not in sight yet. We do note, however, that there is a slight increase in the SST gradient after 2005, which appears to have accelerated over the last few years. While it is difficult to predict the future evolution of the cross-equatorial SST gradient and equatorial Atlantic variability, continued monitoring over the next decade should show in which direction the system is moving.

5. Conclusions

The 2019 positive AZM event was remarkable for its strength and timing. While most AZM events develop in boreal spring and peak in summer, the 2019 event did not develop until mid-fall. Rapid intensification in October and November led to one of the strongest AZM events in the satellite period, thereby terminating a roughly 20-year quiescent interval.

At least two factors contributed to the rapid SST warming: (a) westerly wind anomalies over the central equatorial Atlantic during October and November excited downwelling Kelvin waves that deepened the thermocline in the east; (b) wind stress curl anomalies north of the equator induced downwelling Rossby waves, that were reflected into downwelling equatorial Kelvin waves at the western boundary around September and helped to precondition the equatorial Atlantic. Estimation of the thermodynamic budget in the GODAS ocean reanalysis suggests that upwelling anomalies dominated the warming. The budget analysis, however, cannot quantify which process was

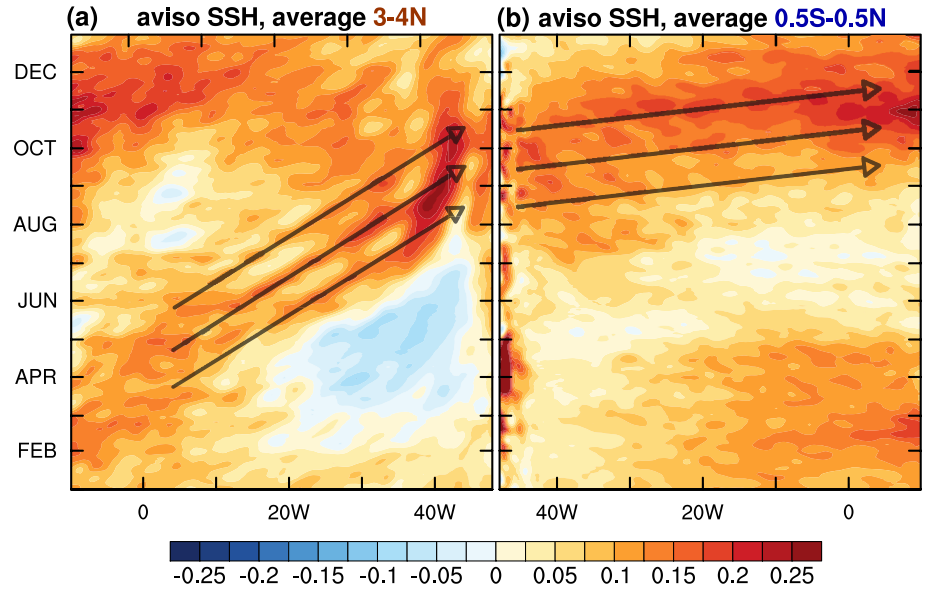

Figure 5. Longitude-time section of AVISO daily mean sea surface height (SSH) anomalies (m) averaged between (a) 3°N and 4°N, and (b) 0.5°S and 0.5°N. The base period is 1993–2012. The arrows indicate the propagation of oceanic Rossby waves in (a) and Kelvin waves in (b). Note that the *x*-axis in (a) has been reversed to help visualize wave reflection at the western boundary.

dominant and is subject to substantial uncertainty due to the absence of large-scale vertical velocity measurements and due to the impact of tropical Atlantic model biases on reanalysis products (Counillon et al., 2021).

Recent studies have suggested that the western Indian Ocean may influence the development of AZM events but, for the 2019 event, we did not find strong evidence for such a pathway. While 2019 did feature an exceptionally strong positive IOD event, the associated precipitation anomalies over the western Indian Ocean became prominent only in October and November. Moreover, daily OLR and wind anomalies are more suggestive of eastward than westward, propagation, hinting at the possibility that the equatorial Atlantic may have contributed to the 2019 positive IOD event. We also did not find strong evidence for a substantial influence of the El Niño Modoki that was ongoing in 2019. Nevertheless, based on the limited analysis presented here, an influence from the Indian and Pacific Oceans cannot be ruled out completely.

Whether the 2019 event marks the end of the 20-year quiescent period remains an open question. It is of interest, however, that another pronounced positive AZM developed in mid-2021 and lasted until December. Provided continued high-quality observations of the equatorial Atlantic, we should be able to tell by the end of the decade whether the equatorial Atlantic is returning to a period of high activity. If so, it would raise questions regarding the ability of climate models to project climate change patterns in the tropical Atlantic and may also have some bearing on the future of other tropical variability modes, such as the IOD and ENSO.

Data Availability Statement

All the datasets used in this study are publicly available. The following lists the datasets and the URLs from which we downloaded them. Registration (free of charge) is required for access to ERA5, JRA-55, and AVISO data. OISST: https://www.ncei.noaa.gov/data/sea-surface-temperature-optimum-interpolation/v2.1/access/avhrr/ HadISST: https://www.metoffice.gov.uk/hadobs/hadisst/data/HadISST_sst.nc.gz COBE SST: https://downloads.psl.noaa.gov/Datasets/COBE/sst.mon.mean.nc ICOADS: https://downloads.psl.noaa.gov/Datasets/icoads/1degree/global/std/sst.mean.nc ERSST: https://www.ncei.noaa.gov/pub/data/cmb/ersst/v5/netcdf/ ERA5: https://cds.climate.copernicus.eu/cdsapp#!/dataset/reanalysis-era5-single-levels-monthly-means?tab=form; hourly data on pressure levels (used in the Supplementary Information) can be found by following the link in the right column under "Related Data" GODAS: https://downloads.psl.noaa.gov/Datasets/godas/ NCEP Reanalysis: https://downloads.psl.noaa.gov/Datasets/ncep/ JRA-55: https://rda.ucar.edu/datasets/ds628.1/ GPCP: https://downloads.

psl.noaa.gov/Datasets/gpcp/precip.mon.mean.nc ePIRATA: http://www.aoml.noaa.gov/phod/epirata/ AVISO: https://cds.climate.copernicus.eu/cdsapp#!/dataset/satellite-sea-level-global?tab=form NOAA OLR: https://downloads.psl.noaa.gov/Datasets/interp_OLR/olr.day.mean.nc

Acknowledgments
We thank the two anonymous reviewers for their helpful comments. This work was supported by the Japan Society for the Promotion of Science KAKENHI, Grant Nos. JP18H01281, JP18H03726, and JP19H05704.

References

Adler, R. F., Huffman, G. J., Chang, A., Ferraro, R., Xie, P., Janowiak, J., et al. (2003). The version 2 global precipitation climatology project (GPCP) monthly precipitation analysis (1979-present). *Journal of Hydrometeorology*, *4*, 1147–1167. https://doi.org/10.1175/1525-7541(2003)004<1147:tvgpcp>2.0.co;2

Ashok, K., Behera, S. K., Rao, S. A., Weng, H., & Yamagata, T. (2007). El Nino Modoki and its possible teleconnection. *Journal of Geophysical Research*, *112*, C11007. https://doi.org/10.1029/2006JC003798

Bjerknes, J. (1969). Atmospheric teleconnections from the equatorial Pacific. *Monthly Weather Review*, *97*, 163–172. https://doi.org/10.1175/1520-0493(1969)097<0163:atftep>2.3.co;2

Bourles, B., Araujo, M., McPhaden, M. J., Brandt, P., Foltz, G. R., Lumpkin, R., et al. (2019). PIRATA: A sustained observing system for tropical Atlantic climate research and forecasting. *Earth and Space Science*, *6*, 577–616. https://doi.org/10.1029/2018EA000428

Burmeister, K., Brandt, P., & Lübbecke, J. F. (2016). Revisiting the cause of the eastern equatorial Atlantic cold event in 2009. *Journal of Geophysical Research:Oceans*, *121*, 4777–4789. https://doi.org/10.1002/2016JC011719

Counillon, F., Keenlyside, N., Toniazzo, T., Koseki, S., Demissie, T., Bethke, I., & Wang, Y. (2021). Relating model bias and prediction skill in the equatorial Atlantic. *Climate Dynamics*, *56*, 2617–2630. https://doi.org/10.1007/s00382-020-05605-8

Doi, T., Behera, S. K., & Yamagata, T. (2020). Predictability of the super IOD event in 2019 and its link with El Niño Modoki. *Geophysical Research Letters*, *47*, e2019GL086713. https://doi.org/10.1029/2019GL086713

Foltz, G. R., & McPhaden, M. J. (2010). Abrupt equatorial wave-induced cooling of the Atlantic cold tongue in 2009. *Geophysical Research Letters*, *37*, L24605. https://doi.org/10.1029/2010gl045522

Foltz, G. R., Schmid, C., & Lumpkin, R. (2018). An enhanced PIRATA dataset for tropical Atlantic ocean-atmosphere research. *Journal of Climate*, *31*, 1499–1524. https://doi.org/10.1175/JCLI-D-16-0816.1

Hu, Z.-Z., & Huang, B. (2007). Physical processes associated with tropical Atlantic SST gradient during the anomalous evolution in the southeastern ocean. *Journal of Climate*, *20*(14), 3366–3378. https://doi.org/10.1175/jcli4189.1

Huang, B., Liu, C., Banzon, V., Freeman, E., Graham, G., Hankins, B., et al. (2021). Improvements of the daily optimum interpolation sea surface temperature (DOISST) version 2.1. *Journal of Climate*, *34*, 2923–2939. https://doi.org/10.1175/JCLI-D-20-0166.1

Imbol Koungue, R. A., Brandt, P., Lübbecke, J., Prigent, A., Martins, M. S., & Rodrigues, R. R. (2021). The 2019 Benguela Niño. *Frontiers in Marine Science*, *8*, 800103. https://doi.org/10.3389/fmars.2021.800103

Keenlyside, N. S., & Latif, M. (2007). Understanding equatorial Atlantic interannual variability. *Journal of Climate*, *20*(1), 131–142. https://doi.org/10.1175/jcli3992.1

Kistler, R., Kalnay, E., Collins, W., Saha, S., White, G., Woollen, J., et al. (2001). The NCEP-NCAR 50-year reanalysis: Monthly means CD-ROM and documentation. *Bulletin of the American Meteorological Society*, *82*, 247–267. https://doi.org/10.1175/1520-0477(2001)082<0247:tnnyrm>2.3.co;2

Kobayashi, S., Ota, Y., Harada, Y., Ebita, A., Moriya, M., Onoda, H., et al. (2015). The JRA-55 Reanalysis: General specifications and basic characteristics. *Journal of Meteorological Society of Japan*, *93*, 5–48. https://doi.org/10.2151/jmsj.2015-001

Liao, H., & Wang, C. (2021). Sea surface temperature anomalies in the western Indian Ocean as a trigger for Atlantic Niño events. *Geophysical Research Letters*, *48*, e2021GL092489. https://doi.org/10.1029/2021GL092489

Liebmann, B., & Smith, C. A. (1996). Description of a complete (interpolated) outgoing longwave radiation dataset. *Bulletin of the American Meteorological Society*, *77*, 1275–1277.

Lübbecke, J. F., Böning, C. W., Keenlyside, N. S., & Xie, S.-P. (2010). On the connection between Benguela and equatorial Atlantic Niños and the role of the South Atlantic anticyclone. *Journal of Geophysical Research*, *115*, C09015. https://doi.org/10.1029/2009JC005964

Lübbecke, J. F., & McPhaden, M. J. (2012). On the inconsistent relationship between pacific and Atlantic Niños. *Journal of Climate*, *25*, 4294–4303.

Martín-Rey, M., Polo, I., Rodríguez-Fonseca, B., Losada, T., & Lazar, A. (2018). Is there evidence of changes in tropical Atlantic variability modes under AMO phases in the observational record? *Journal of Climate*, *32*(2), 515–536.

Merle, J. (1980). Annual and interannual variability of temperature in the eastern equatorial Atlantic Ocean – Hypothesis of an Atlantic El Nino. *Oceanologica Acta*, *3*, 209–220.

Nnamchi, H. C., Latif, M., Keenlyside, N. S., Kjellsson, J., & Richter, I. (2021). Diabatic heating governs the seasonality of the Atlantic Niño. *Nature Communications*, *12*, 376. https://doi.org/10.1038/s41467-020-20452-1

Nnamchi, H. C., Li, J., Kucharski, F., Kang, I., Keenlyside, N. S., Chang, P., & Farneti, R. (2016). An equatorial–extratropical dipole structure of the Atlantic Niño. *Journal of Climate*, *29*, 7295–7311. https://doi.org/10.1175/JCLI-D-15-0894.1

Okumura, Y., & Xie, S. P. (2004). Interaction of the Atlantic equatorial cold tongue and the African monsoon. *Journal of Climate*, *17*, 3589–3602. https://doi.org/10.1175/1520-0442(2004)017<3589:IOTAEC>2.0.CO;2

Okumura, Y., & Xie, S.-P. (2006). Some overlooked features of tropical Atlantic climate leading to a New Niño-like phenomenon. *Journal of Climate*, *19*, 5859–5874. https://doi.org/10.1175/jcli3928.1

Prigent, A., Lübbecke, J. F., Bayr, T., Latif, M., & Wengel, C. (2020). Weakened SST variability in the tropical Atlantic ocean since 2000. *Climate Dynamics*, *54*, 2731–2744. https://doi.org/10.1007/s00382-020-05138-0

Richter, I., Behera, S. K., Masumoto, Y., Taguchi, B., Komori, N., & Yamagata, T. (2010). On the triggering of Benguela Niños: Remote equatorial versus local influences. *Geophysical Research Letters*, *37*, L20604. https://doi.org/10.1029/2010GL044461

Richter, I., Behera, S. K., Masumoto, Y., Taguchi, B., Sasaki, H., & Yamagata, T. (2013). Multiple causes of interannual sea surface temperature variability in the equatorial Atlantic Ocean. *Nature Geoscience*, *6*, 43–47. https://doi.org/10.1038/ngeo1660

Richter, I., & Tokinaga, H. (2020). An overview of the performance of CMIP6 models in the tropical Atlantic: Mean state, variability, and remote impacts. *Climate Dynamics*, *55*(9), 2579–2601. https://doi.org/10.1007/s00382-020-05409-w

Richter, I., & Tokinaga, H. (2021). The Atlantic zonal mode: Dynamics, thermodynamics, and teleconnections. In S. K. Behera (Ed.), *Tropical and extratropical air-sea interactions*. Elsevier. https://doi.org/10.1016/b978-0-12-818156-0.00008-3

Richter, I., Xie, S.-P., Morioka, Y., Doi, T., Taguchi, B., & Behera, S. K. (2017). Phase locking of equatorial Atlantic variability through the seasonal migration of the ITCZ. *Climate Dynamics*, *48*, 3615–3629. https://doi.org/10.1007/s00382-016-3289-y

Saji, N. H., Goswami, B. N., Vinayachandran, P. N., & Yamagata, T. (1999). A dipole mode in the Indian Ocean. *Nature*, *401*, 360–363. https://doi.org/10.1038/43854

Servain, J., Caniaux, G., Kouadio, Y. K., McPhaden, M. J., & Araujo, M. (2014). Recent climatic trends in the tropical Atlantic. *Climate Dynamics*, *43*, 3071–3089. https://doi.org/10.1007/s00382-014-2168-7

Servain, J., Wainer, I., McCreary, J. P., & Dessier, A. (1999). Relationship between the equatorial and meridional modes of climatic variability in the tropical Atlantic. *Geophysical Research Letters*, *26*, 485–488. https://doi.org/10.1029/1999GL900014

Tokinaga, H., & Xie, S.-P. (2011). Weakening of the equatorial Atlantic cold tongue over the past six decades. *Nature Geoscience*, *4*, 222–226. https://doi.org/10.1038/ngeo1078

Vallès-Casanova, I., Lee, S.-K., Foltz, G. R., & Pelegrí, J. L. (2020). On the spatiotemporal diversity of Atlantic Niño and associated rainfall variability over West Africa and South America. *Geophysical Research Letters*, *47*, 087108.

Zebiak, S. E., & Cane, A. (1987). A model El Niño-Southern oscillation. *Monthly Weather Review*, *115*, 2262–2278. https://doi.org/10.1175/1520-0493(1987)115<2262:ameno>2.0.co;2

Zhang, L., & Han, W. (2021). Indian Ocean Dipole leads to Atlantic Niño. *Nature Communications*, *12*, 5952. https://doi.org/10.1038/s41467-021-26223-w

References From the Supporting Information

Enfield, D. B., Mestas-Nunez, A. M., & Trimble, P. J. (2001). The Atlantic Multidecadal Oscillation and its relationship to rainfall and river flows in the continental U.S. *Geophysical Research Letters*, *28*, 2077–2080.

Frajka-Williams, E., Beaulieu, C., & Duchez, A. (2017). Emerging negative Atlantic Multidecadal Oscillation index in spite of warm subtropics. *Scientific Reports*, *7*, 11224. https://doi.org/10.1038/s41598-017-11046-x

Freeman, E., Woodruff, S. D., Worley, S. J., Lubker, S. J., Kent, E. C., Angel, W. E., et al. (2016). ICOADS Release 3.0: A major update to the historical marine climate record. *International Journal of Climatology*, *37*, 2211–2232. https://doi.org/10.1002/joc.4775

Hersbach, H., Bell, B., Berrisford, P., Hirahara, S., Horanyi, A., Munoz-Sabater, J., et al. (2020). The ERA5 global reanalysis. *Quarterly Journal of the Royal Meteorological Society*, 1–51. https://doi.org/10.1002/qj.3803

Huang, B., Thorne, P. W., Banzon, V. F., Boyer, T., Vose, R. S., Chepurin, G., et al. (2017). Extended reconstructed sea surface temperature version 5 (ERSSTv5), upgrades, validations, and intercomparisons. *Journal of Climate*, *30*, 8179–8205. https://doi.org/10.1175/JCLI-D-16-0836.1

Ishii, M., Shouji, A., Sugimoto, S., & Matsumoto, T. (2005). Objective analyses of sea-surface temperature and marine meteorological variables for the 20th century using ICOADS and the kobe collection. *International Journal of Climatology*, *25*, 865–879. https://doi.org/10.1002/joc.1169

Rayner, N. A., Parker, D. E., Horton, E. B., Folland, C. K., Alexander, L. V., Rowell, D. P., et al. (2003). Global analyses of sea surface temperature, sea ice, and night marine air temperature since the late nineteenth century. *Journal of Geophysical Research*. Vol. *108*(D14), 4407. https://doi.org/10.1029/2002JD002670

Saha, S., Nadiga, S., Thiaw, C., Wang, J., Wang, W., Zhang, Q., et al. (2006). The NCEP climate forecast system. *Journal of Climate*, *19*(15), 3483–3517. https://doi.org/10.1175/JCLI3812.1

Trenberth, K. E., & Shea, D. J. (2006). Atlantic hurricanes and natural variability in 2005. *Geophysical Research Letters*, *33*, L12704. https://doi.org/10.1029/2006GL026894

Wheeler, M., & Kiladis, G. N. (1999). Convectively coupled equatorial waves: Analysis of clouds and temperature in the wavenumber-frequency domain. *Journal of the Atmospheric Sciences*, *56*, 374–399.